Acta Mech 228, 1793–1817 (2017)
DOI 10.1007/s00707-016-1793-0

ORIGINAL PAPER

Iman Karimipour · Ali Reza Fotuhi

Anti-plane analysis of an infinite plane with multiple cracks based on strain gradient theory

Received: 21 August 2015 / Revised: 28 July 2016 / Published online: 19 January 2017

Abstract The anti-plane stress analysis in an infinite elastic isotropic plane is carried out by using the distributed dislocation techniques in the framework of strain gradient theory. The technique involves the solution of a screw Volterra dislocation in the region. Employing a distributed dislocation solution indicated that the stress components reveal the familiar hypersingularity at the site of the dislocation. The solution for stress fields in integral form is obtained for a plane containing a Volterra-type screw dislocation via Fourier transform of the biharmonic equation. This method is extended to allow the solution of integral equations in the regions weakened by multiple smoothed curved cracks under anti-plane deformation. The integral equations are solved numerically for the density of dislocation on the crack surfaces. The numerical method in Chebyshev series forms is used to solve the hypersingular integral equations. The effects of interaction among cracks with different arrangements and those of the size effect on the stress intensity factors are discussed. To confirm the validity of the formulations, numerical values of the results are compared. The predicted results via the aforementioned approach are in excellent agreement with those in the literature. Some new examples are solved to demonstrate the applicability of the procedure.

1 Introduction

In many structures, crack creation is one of the most significant fracture mechanisms. To predict these fracture mechanisms, accurate modeling is necessary [1]. Nowadays, synthesis and manipulation of materials on a nano-scale, which lead to the fabrication of innovative materials suitable for certain behaviors, have increasingly gained attention on the part of a good number of scientists and engineers during the past decade. An accurate description of the behavior of nano-material requires consideration of its pertinent nano-structural features [2–4].

Some studies on the behavior of materials in macro-scales have been carried out by previous researchers during the previous decade. But these studies have not been done at nano-scale [5–8]. By decreasing the dimensions to sub-micron, the nano-scale phenomena (length effect) emerge, which should be taken into account in theoretical models [9–11]. The important phenomenon in nano-scale is size-dependency of the mechanical performance of nano-structures. It shows itself significantly in the deformation tests of microstructures [9].

Due to the discrete nature of materials at atomic scale, the size-dependent behavior of materials and structures at sub-micron distances cannot be modeled using classical continuum mechanics [12]. Furthermore, this method has some innate weaknesses since it proposes physically unrealistic singularities, which appear in the strain and stress fields in the vicinity of such defects as dislocations and cracks. On the other hand, usual

I. Karimipour · A. R. Fotuhi (✉)
Department of Mechanical Engineering, Yazd University, Safaeieh, Yazd, Iran
E-mail: afotuhi@yazd.ac.ir
Tel.: +98-35-31232499
Fax: +98-35-38212781

continuum theory fails to give an accurate solution near the crack tip. Moreover, it implies that a solid is able to sustain an infinite stress at the Griffith–Inglis crack tips.

As a remedy to deal with the above problems, various enriched theories have been proposed in the literature. In this regard, non-local elasticity [13], Cosserat continuum theory [2], strain gradient elasticity [14], couple stress theory [15,16], and simulation technics such as molecular dynamics (MD), which are widely used in monitoring the behavior of a specific system of atoms during dynamic processes [17], have been developed to incorporate the size effect into theoretical models. These methods are widely employed in the nano-scale studies of thin films, nano-composites, nano-beams and quantum dots, among others [18–21].

In the strain gradient theory, the second-order deformation gradient tensor is used [22]. Mindlin [23,24] established strain gradient and couple stress theory to enable continuum theories to consider size effects. Mindlin also [25] employed couple stress theory to determine the stress concentration factor of circular and spherical holes, which have only one characteristic length. Lubarda [26] presented a solution pertinent to inclusions, voids, and inhomogeneities in anti-plane strain problems with couple stress. Shodja and Ghazisaedi [27] applied the couple stress theory to the anti-plane problems in piezoelectric media containing a circular void or a circular piezoelectric inhomogeneity. Haftbaradaran and Shodja [28] considered elliptical inclusions and inhomogeneities subjected to uniform far-field anti-plane shear stress via couple stress theory to study the stress and strain fields of elliptic inhomogeneities. Zhang et al. [29] employed strain gradient elasticity to study the interactions between defects within graphene. They observed that in the vicinity of a defect the results of gradient elasticity are in line with those of semi-empirical quantum mechanics, whereas the solution of classical elasticity becomes inaccurate as the defect line is approached. Shodja and Tehranchi [30] evaluated the length scales associated with the first gradient theory for various FCC metals and compared the elastic fields of a nano-void as predicted by the gradient theory with those obtained by atomic simulation. Shodja et al. [31] used a simplified version of strain gradient elasticity for an accurate determination of the displacement, strain, and stress fields of a screw dislocation in a nanowire. Davoudi et al. [32] used a more elaborated version of strain gradient elasticity to analyze the stress field of the nanowire.

Aifantis in his work developed non-singular close-form solutions for the stress and strain fields, which vanish as the crack tip is approached. He presented expressions that are convenient to use for revisiting many engineering problems in the field of LEFM and for checking their validity [33].

The gradient (Laplacian enriched) expressions for the stress and strain fields were derived and discussed in [34] where a comparison with Eringen's non-local elasticity theory was made. A further discussion on the physical meaning of these non-singular solutions for the (micro) stresses and (micro) strains at the crack tip and their consistency with experimental observations was presented in [35] where some misunderstandings and rather misleading statements on equilibrium and compatibility -readily satisfied by the conventional (macro)stress and (macro)strain fields- appearing in the Literature [36] were pointed out.

Lazar and Polyzos [36] studied the physical meaning and the rendition of the non-singular stress and strain fields of the tip cracks in LEFM. They claimed that the proposed solutions convince the equilibrium, boundary, and compatibility conditions. This treatment should be regarded together with the challenge between the works of these authors with publishing some articles of Aifantis such as Ref. [34] (and at the following Ref. [52]), along with a "Comment" by Aifantis that criticizes their article. For answer to the Aifantis Comment, Lazar and Polyzos by publishing the article "On gradient enriched elasticity theories: A reply to "Comment on 'On non-singular crack fields in Helmholtz type enriched elasticity theories" and important theoretical aspects" by means of acquit and aboveboard arguments could dispute Aifantis' Comment.

Gutkin and Aifantis employed screw dislocation in gradient elasticity. The main purpose of their work was to eliminate the elastic strain singularity at the dislocation line [37].

The physical meaning and style of the strain gradient terms for whole of the materials, along with the nature of material behavior, was studied by Aifantis [38].

The physical meaning, implications, and general behavior of size-dependent phenomena of non-classical theory can be better understood from the "Appendix A". Also it should be mentioned that an attracting and rather conclusive treatment on the origin and physical meaning of non-singular crack-tip solutions for strains and stresses in strain gradient theory can be establish in a new manuscript from Aifantis [35].

The determination of the stress intensity factor (SIF) at the tip of the nano-crack has also been taken up with a particular interest. Recently, Paulino et al. [39] examined the problem of a crack perpendicular to the direction of material gradation of FGM plane based on anisotropic strain gradient elasticity theory. The stress intensity factor in an FGM plane containing a crack parallel to the material gradation was obtained by Chan et al. [40] with anisotropic strain gradient elasticity. In the above works, the sensitivity of the stress intensity

factor to size effects was demonstrated. Georgiadis [41] investigated the elastic stress and displacement fields around a crack by drawing upon the dipolar gradient theory.

While some size effect models based on strain gradient have been used to calculate SIF, few researches have utilized strain gradient theory for analyzing media with multiple defects. One of the first works in this field has been conducted by Paulino et al. [39] who calculated the SIF of an infinite plane using strain gradient elasticity theory. However, they did not consider the effects of multiple cracks in their models. Other researches have been addressed in [42–47]. It should be mentioned that all of the above works have been conducted on SIF of a plane with a single crack. Indeed, while the stress intensity factor of such a plane has been widely addressed in the literature, few studies have been dedicated to modeling this plane with multiple defects.

To the best knowledge of the authors, as it is observed, the stress intensity factor of a plane incorporating both influences of size effects and interaction among multiple cracks with different geometry has not hitherto been investigated in the previous researches. Hence, in this work, the infinite plane under anti-plane deformations weakened via multiple defects is considered to scrutinize the influence of the nano-scale phenomena on the behavior of the plane, also the material in nano-scale is modeled by considering the strain gradient elasticity and is analytically implemented by a dislocation approach to calculate the stress intensity factor. The obtained results are quite plausible compared with those in the literature.

2 Fundamentals of strain gradient theory

In Mindlin's work [23], the strain energy density function is expressed as a function of strain ε_{ij} and strain gradient $\varepsilon_{ij,k}$ for a linear, elastic, and isotropic material, respectively. It is worth mentioning that the theory used in the present work, introduced by Casal [43], is a special case of a Mindlin-type with two non-classical length scale parameters relevant to volume (internal length (L)) and surface strain gradient elastic energy contribution tensors (director length ($L^{'}$)) that affect the behavior of nano-structures [48]. Although in Mindlin-type 2nd, fully presented in [49], along with what was mentioned above, rotation gradients are in the strain energy density. Often, for simplicity and reduction in the number of material length scale constants, these parameters can be regarded as only one single measurable parameter (rotation gradient) under the assumptions of couple stress theory [50]. Altan and Aifantis, and Ru and Aifantis [51,52], proposed the gradient elasticity with only one material constant. This assumption may also be beneficial for experimental measurements.

Regarding the strain gradient theory modified and suggested by Casal [43], U as the strain energy density function in the linear elastic and isotropic material is written as follows:

$$U = \frac{1}{2}\lambda\varepsilon_{ii}\varepsilon_{jj} + G\varepsilon_{ij}\varepsilon_{ji} + GL^2\kappa_{kij}\kappa_{kji} + GL^{'}\left(\kappa_{kij}\varepsilon_{ji} + \varepsilon_{ij}\kappa_{kji}\right) \tag{1}$$

where

$$\varepsilon_{ij} = \frac{1}{2}\left(u_{i,j} + u_{j,i}\right), \quad \kappa_{ijk} = \partial_i\varepsilon_{jk}, \quad \lambda = E\upsilon/\left(1+\upsilon\right)\left(1-2\upsilon\right), \quad G = E/2\left(1+\upsilon\right). \tag{2}$$

In the above equations, u_i, ε_{ij}, κ_{ijk}, λ, and G indicate components of displacement vector, the infinitesimal strain and strain gradient, Lame constant, and shear modulus, respectively. The last two terms in Eq. (1) are corresponsive with surface energy. It should be noted that the following result was obtained in a special case. Letting $L^{'} = L = 0$, the relations are simplified to those obtained by classic continuum theory. The selected size of the parameter variation ($L^{'}$, L) is chosen based on the sensitivity of the parameter to strain energy density, as $\left|L^{'}/L\right| < 1, L \neq 0$, and $3\lambda + 2G > 0$ because the strain energy density function needs to be non-negative [23]. Work conjugates of strain and strain gradient with constitutive relation for the gradient elasticity are identified as follows [39]:

$$\tau_{ij} = \frac{\partial U}{\partial\varepsilon_{ij}} = \lambda\varepsilon_{kk}\delta_{ij} + 2G\varepsilon_{ij} + 2GL^{'}\kappa_{kij}, \quad \mu_{ijk} = \frac{\partial U}{\partial\kappa_{ijk}} = 2GL^2\kappa_{ijk} + 2GL^{'}\varepsilon_{jk},$$
$$\sigma_{jk} = \tau_{jk} - \partial_i\mu_{ijk} = \lambda\varepsilon_{ii}\delta_{jk} + 2G\left(1 - L^2\nabla^2\right)\varepsilon_{jk}. \tag{3}$$

In the above equation ∇^2 denotes the Laplacian operator, δ_{jk} is the Kronocker delta, τ_{ij} is symmetric in indices i and j, and μ_{ijk} is symmetric in indices j and k. τ_{ij}, μ_{ijk}, and σ_{ij} are components of Cauchy's stress, high-order stress tensors, and total stresses, respectively. By neglecting body force, the equations of motion in static equilibrium in the framework of strain gradient theory are obtained as $(\lambda + 2G)(1 - L^2\nabla^2)\nabla\nabla.w = 0$ [39].

2.1 Plane with screw dislocation

Under conditions of anti-plane deformation, the only non-zero component of the displacement is the out-of-plane component $w(x, y)$. The displacement field is stated as follows:

$$u = v = 0, \quad w = w\,(x, y)\,. \tag{4}$$

In the above equation (4), u, v, and w indicate displacement in the direction of the x, y, and z axis, respectively. Consequently, the constitutive relationships and components of stress and double stress in strain gradient theory read as [39]:

$$\sigma_{yz} = 2G(\varepsilon_{yz} - L^2\nabla^2\varepsilon_{yz}) = G\left(\frac{\partial w}{\partial y}\right) - GL^2\left(\frac{\partial^3 w}{\partial y^3} + \frac{\partial^3 w}{\partial y \partial x^2}\right), \tag{5.1}$$

$$\sigma_{xz} = 2G(\varepsilon_{xz} - L^2\nabla^2\varepsilon_{xz}) = G\left(\frac{\partial w}{\partial x}\right) - GL^2\left(\frac{\partial^3 w}{\partial x^3} + \frac{\partial^3 w}{\partial x \partial y^2}\right), \tag{5.2}$$

$$\mu_{yyz} = 2G\left(L^2\frac{\partial}{\partial y}\varepsilon_{yz} - L^{'}\varepsilon_{yz}\right) = GL^2\frac{\partial^2 w}{\partial y^2} - GL^{'}\frac{\partial w}{\partial y}. \tag{6}$$

The equilibrium equation in strain gradient theory may be written as [39]:

$$\frac{\partial \sigma_{xz}}{\partial x} + \frac{\partial \sigma_{yz}}{\partial y} = 0. \tag{7}$$

Substituting (5.1) into Eq. (7), one can obtain an equation in terms of displacement as follows:

$$\nabla^2 w - L^2\nabla^4 w = 0. \tag{8}$$

Equation (8) is solved by means of the complex Fourier transform. The complex Fourier transformation is defined as:

$$f^*(\xi) = \int_{-\infty}^{\infty} f(x)\mathrm{e}^{i\xi x}\mathrm{d}x \tag{9}$$

where $i = \sqrt{-1}$. The inversion of (9) is:

$$f(x) = \frac{1}{2\pi}\int_{-\infty}^{\infty} f^*(\xi)\mathrm{e}^{i\xi x}\mathrm{d}\xi. \tag{10}$$

Applying Fourier transform (9) to Eq. (8), the following result is gained:

$$L^2\frac{\mathrm{d}^4 w^*\,(\xi, y)}{\mathrm{d}y^4} - \left(2L^2\xi^2 + 1\right)\frac{\mathrm{d}^2 w^*\,(\xi, y)}{\mathrm{d}y^2} + \left(L^2\xi^4 + \xi^2\right)w^*\,(\xi, y) = 0. \tag{11}$$

In Eq. (11), $w^*\,(\xi, y)$ is the Fourier transform of the displacement field. Solving the resultant equation (11) and in conjunction with the property of decaying behavior of displacement components as $|y| \to \infty$ we arrive at:

$$w^*\,(\xi, y) = A\,(\xi)\,e^{-|\xi|y} + B\,(\xi)\,e^{-\sqrt{\xi^2 + \frac{1}{L^2}}y}. \tag{12}$$

In the above equation, $A(\xi)$ and $B(\xi)$ are unknown. We consider an infinite plane (Fig. 1) made up of isotropic material, where G is the elastic shear modulus.

Let a Volterra-type screw dislocation with Burgers vector b_z be situated in the plane. The dislocation line is depicted in Fig. 1. The conditions representing the dislocation and stress continuity are:

$$w\left(x, 0^+\right) - w\left(x, 0^-\right) = b_z H(x), \quad \sigma_{yz}\left(x, 0^+\right) = \sigma_{yz}\left(x, 0^-\right), \quad \mu_{yyz}\left(x, 0^+\right) = \mu_{yyz}\left(x, 0^-\right) \tag{13.1–3}$$

In the above relation, $H(x)$ is the Heaviside-step function. Equation (13.1) enforces the multivaluedness of displacement, while (13.2) and (13.3) imply the continuity of traction along the dislocation line. Due to the symmetry of geometry and antisymmetric loading condition, only the upper-half of the plane has been

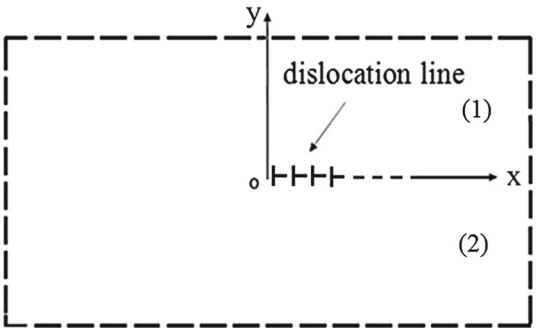

Fig. 1 Schematic view of a plane with a screw dislocation

modeled. Therefore, we continue our discussion based on boundary condition and stress continuity in the following manner:

$$w\,(x,0) = \frac{1}{2} b_z H(x), \tag{14}$$

$$\mu_{yyz}\,(x,0) = 2G\left(L^2\frac{\partial \varepsilon_{yz}}{\partial y} - L^{'}\varepsilon_{yz}\right)\Big|_{y=0} = G\left(L^2\frac{\partial^2 w}{\partial y^2} - L^{'}\frac{\partial w}{\partial y}\right)\Big|_{y=0} = 0. \tag{15}$$

The Fourier transform of (14) and (15) by virtue of (9) results in:

$$w^* = \frac{1}{2} b_z \left(\pi\delta(\xi) + \frac{i}{\xi}\right), \tag{16}$$

$$\mu^*_{yyz}\,(x,0) = GL^2\frac{d^2 w^*\,(\xi,y)}{\mathrm{d}y^2} - GL^{'}\frac{\mathrm{d}w^*\,(\xi,y)}{\mathrm{d}y}\Big|_{y=0} = 0. \tag{17}$$

In the above relation $\delta(s)$ is the Dirac delta function. By substituting $A(\xi)$ and $B(\xi)$ with (12) and applying the Fourier transform inversion formula (10), the displacement field in the infinite plane is yielded as [46]:

$$\begin{aligned} w(x,y) = {} & \frac{b_z}{4\pi}, \\ & \times \int_{-\infty}^{\infty} \left(\frac{-\left(\pi\delta\left(\xi\right)\xi + i\right)\left(L^3\xi^2 + L + L^{'}\sqrt{1+L^2\xi^2}\right)}{\left(LL^{'}\left|\xi\right| - L - L^{'}\sqrt{1+L^2\xi^2}\right)\xi} \mathrm{e}^{-|\xi|y} \right. \\ & \left. + \frac{\left(\pi\delta\left(\xi\right)\xi + i\right)\left(L^3\xi^2 + LL^{'}\left|\xi\right|\right)}{\left(LL^{'}\left|\xi\right| - L - L^{'}\sqrt{1+L^2\xi^2}\right)\xi} \mathrm{e}^{-\sqrt{\xi^2+\frac{1}{L^2}}y} \right) \mathrm{e}^{-ix\xi}\mathrm{d}\xi. \end{aligned} \tag{18}$$

The stress components in view of (5.1) and (5.2) with (18) may be expressed as:

$$\sigma_{xz} = \frac{-iG}{2\pi}\int_{-\infty}^{\infty} \xi A(\xi)\mathrm{e}^{-|\xi|y}\mathrm{e}^{-ix\xi}\mathrm{d}\xi, \quad \sigma_{yz} = \frac{-G}{2\pi}\int_{-\infty}^{\infty} |\xi|\, A(\xi)\mathrm{e}^{-|\xi|y}\mathrm{e}^{-ix\xi}\mathrm{d}\xi. \tag{19}$$

Using the property of the Dirac delta function and splitting the integrals in (19) into odd and even parts with respect to the parameter ξ and after some manipulation, the stress fields are written as:

$$\begin{aligned} \sigma_{xz} &= \frac{-Gb_z}{2\pi}\int_0^{\infty} \kappa\,(\xi)\,\mathrm{e}^{-\xi y}\cos\left(x\xi\right)\mathrm{d}\xi, \\ \sigma_{yz} &= \frac{Gb_z}{2\pi}\int_0^{\infty} \kappa\,(\xi)\,e^{-\xi y}\sin\left(x\xi\right)\mathrm{d}\xi, \quad \kappa\,(\xi) = \frac{L^3\xi^2 + L + L^{'}\sqrt{1+L^2\xi^2}}{LL^{'}\xi - L - L^{'}\sqrt{1+L^2\xi^2}}. \end{aligned} \tag{20}$$

In order to specify the singularity of the stress components, the asymptotic behavior of the integrands in (20) should be examined. Since the integrands are continuous functions of ξ and also finite at $\xi = 0$, the singularity must occur as ξ tends to infinity. An asymptotic analysis allows splitting of the kernel $\kappa(\xi)$ into the singular $\kappa_\infty(\xi) = \lim_{|\xi|\to\infty} \kappa(\xi)$ and non-singular parts: $\kappa(\xi) = \kappa_\infty(\xi) + [\kappa(\xi) - \kappa_\infty(\xi)]$ and $\kappa_\infty(\xi) = -L^2\xi^2 - \frac{1}{2}L'\xi - 1 + \left(L'/2L\right)^2$. By virtue of the following identities:

$$\begin{aligned}
&\int_0^\infty e^{-\xi|y|}\cos(x\xi)d\xi = \frac{|y|}{r^2}, \int_0^\infty \xi e^{-\xi|y|}\cos(x\xi)d\xi = \frac{y^2-x^2}{r^4},\\
&\int_0^\infty \xi^2 e^{-\xi|y|}\cos(x\xi)d\xi = \frac{-2|y|(3x^2-y^2)}{r^6}, \int_\infty^0 e^{-\xi|y|}\sin(x\xi)d\xi = \frac{x}{r^2},\\
&\int_0^\infty \xi e^{-\xi|y|}\sin(x\xi)d\xi = \frac{2|y|x}{r^4}, \int_0^\infty \xi^2 e^{-\xi|y|}\sin(x\xi)d\xi = -\frac{2x(x^2-3y^2)}{r^6},
\end{aligned} \tag{21}$$

the stress fields in the entire region read

$$\begin{aligned}
\sigma_{xz} = \frac{Gb_z}{2\pi} \times \Bigg\{ &\left(1 - \left(\frac{L'}{2L}\right)^2\right)\frac{|y|}{r^2}\\
&+ \frac{\mathrm{sgn}(y)\,L'\left(y^2-x^2\right)}{2r^4} + \frac{2L^2|y|\left(y^2-3x^2\right)}{r^6}\\
&- \mathrm{sgn}(y)\int_0^\infty (\kappa(\xi) - \kappa_\infty(\xi))\, e^{-\xi|y|}\cos(x\xi)d\xi \Bigg\},\\
\sigma_{yz} = \frac{Gb_z}{2\pi}\\
&\times \Bigg\{ \left(\left(\frac{L'}{2L}\right)^2 - 1\right)\frac{x}{r^2} - \frac{L'\mathrm{sgn}(y)|y|x}{r^4} + \frac{2L^2x\left(x^2-3y^2\right)}{r^6}\\
&+ \int_0^\infty (\kappa(\xi) - \kappa_\infty(\xi))\, e^{-\xi|y|}\sin(x\xi)d\xi \Bigg\}.
\end{aligned} \tag{22}$$

In the above equations $r^2 = x^2 + y^2$ is the distance from the dislocation site. Equation (22) reveals that the stress fields are Cauchy type as well as hypersingular at the dislocation position. Moreover, the integrands in (22) decay quite rapidly as $\xi \to \infty$, which makes the integrals susceptible to numerical evaluation.

It can be seen that as L and L' tend to be zero or the effects of the characteristic length vanish in (22), these equations are reduced to those of the classic theory.

3 Crack formulation

The dislocation solutions accomplished in the preceding Section may be employed to analyze the plane and to derive the integral equations for the crack problem, with several arbitrarily oriented cracks. The stress components caused by a screw dislocation located at (x_0, y_0) with dislocation line parallel to the x-axis may be written from Eq. (22) as [53,54]:

$$\sigma_{xz} = \frac{Gb_z}{2\pi} \times \left\{ \left(1 - \left(\frac{L'}{2L} \right)^2 \right) \frac{(y-y_0)}{r_1^2} + \frac{L'}{2} \frac{(y-y_0)^2 - (x-x_0)^2}{r_1^4} + \frac{2L^2 (y-y_0)\left((y-y_0)^2 - 3(x-x_0)^2\right)}{r_1^6} - \int_0^\infty (\kappa(\xi) - \kappa_\infty(\xi)) e^{-\xi(y-y_0)} \cos((x-x_0)\xi) d\xi \right\} \text{ for } y_0 \le y,$$

$$\sigma_{xz} = \frac{Gb_z}{2\pi} \times \left\{ \left(1 - \left(\frac{L'}{2L} \right)^2 \right) \frac{(y-y_0)}{r_1^2} - \frac{L'}{2} \frac{(y-y_0)^2 - (x-x_0)^2}{r_1^4} + \frac{2L^2 (y-y_0)\left((y-y_0)^2 - 3(x-x_0)^2\right)}{r_1^6} + \int_0^\infty (\kappa(\xi) - \kappa_\infty(\xi)) e^{\xi(y-y_0)} \cos((x-x_0)\xi) d\xi \right\} \text{ for } y < y_0,$$

$$\sigma_{yz} = \frac{Gb_z}{2\pi} \times \left\{ \left(\left(\frac{L'}{2L} \right)^2 - 1 \right) \frac{(x-x_0)}{r_1^2} - \frac{L'(y-y_0)(x-x_0)}{r_1^4} + \frac{2L^2 (x-x_0)\left((x-x_0)^2 - 3(y-y_0)^2\right)}{r_1^6} + \int_0^\infty (\kappa(\xi) - \kappa_\infty(\xi)) e^{-\xi(y-y_0)} \sin((x-x_0)\xi) d\xi \right\} \text{ for } y_0 \le y,$$

$$\sigma_{yz} = \frac{Gb_z}{2\pi} \times \left\{ \left(\left(\frac{L'}{2L} \right)^2 - 1 \right) \frac{(x-x_0)}{r_1^2} + \frac{L'(y-y_0)(x-x_0)}{r_1^4} + \frac{2L^2 (x-x_0)\left((x-x_0)^2 - 3(y-y_0)^2\right)}{r_1^6} + \int_0^\infty (\kappa(\xi) - \kappa_\infty(\xi)) e^{\xi(y-y_0)} \sin((x-x_0)\xi) d\xi \right\} \text{ for } y < y_0. \quad (23)$$

In the above relation $r_1^2 = (x-x_0)^2 + (y-y_0)^2$, and Eq. (23) can be stated as Eq. (24):

$$\sigma_{jz}(x, y) = b_z \times \begin{cases} k_{jz}^1(x, y, x_0, y_0), y_0 \le y \\ k_{jz}^2(x, y, x_0, y_0), y < y_0 \end{cases}, j = x, y \quad (24)$$

where $k_{jz}^l(x, y, x_0, y_0), l = 1, 2, j = x, y$ in Eq. (24) are the coefficients of b_z and may be deduced from (23). In order to solve the problem of the crack of arbitrary orientation, it is essential to appraise the shear stresses along the line of the surface crack in terms of a dislocation with Burgers vector in a coordinate system local to the crack. The former solution is applicable wherever the line joining the dislocation site and the point under consideration on the crack surface is parallel to the dislocation line (x-axis), whereas another solution should be chosen otherwise.

Equation (22) may be recast to more appropriate forms, for this purpose the coordinate axes local to the crack (X,Y), are oriented at an angle θ to the global axes(x,y), where θ is measured from the positive x-axis counterclockwise.

Now we need the stresses due to a dislocation placed at an arbitrary position (θ), Fig. 2.

Let the locations of the dislocation be $(x_0, y_0) = (\alpha(s), \beta(s))$ with a sidling angle θ as shown in Fig. 2, and the screw dislocation with density $b_z(s)$ is distributed on a surface crack, so that the local stress

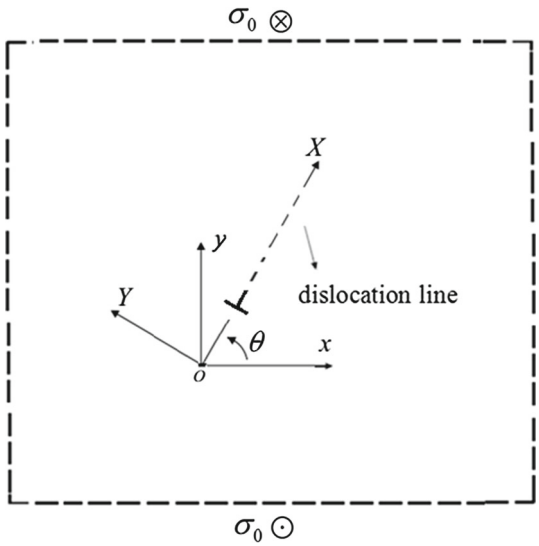

Fig. 2 Schematic view of a plane with a screw dislocation at a crooked angle

field σ_{Xz}, σ_{Yz} may be written in terms of the local coordinates (X, Y) after rotation by substituting $X = (x - \alpha(s))\cos(\theta) + (y - \beta(s))\sin(\theta)$, $Y = (y - \beta(s))\cos(\theta) - (x - \alpha(s))\sin(\theta)$ in Eq. (22) [55]. The stress components on the local coordinates X–Y as seen in Fig. 2, located on the surface of the crack in terms of the stress components in x–y coordinates, become [56]:

$$\begin{aligned}
\sigma_{\mathrm{Xz}} = \frac{G}{2\pi}\int_{-1}^{1} b_z(s)\sqrt{\left[\alpha'(s)\right]^2+\left[\beta'(s)\right]^2}\times\Bigg\{&\left(1-\left(\frac{L'}{2L}\right)^2\right)\frac{|(y-\beta(s))\cos(\theta)-(x-\alpha(s))\sin(\theta)|}{r_2^2}\\
&+\frac{L'}{2}\mathrm{sgn}\left((y-\beta(s))\cos(\theta)-(x-\alpha(s))\sin(\theta)\right)\\
&\times\frac{((y-\beta(s))\cos(\theta)-(x-\alpha(s))\sin(\theta))^2-((x-\alpha(s))\cos(\theta)+(y-\beta(s))\sin(\theta))^2}{r_2^4}\\
&+\{|(y-\beta(s))\cos(\theta)-(x-\alpha(s))\sin(\theta)|\}\\
&\times\left[2L^2\frac{\left(((y-\beta(s))\cos(\theta)-(x-\alpha(s))\sin(\theta))^2-3((x-\alpha(s))\cos(\theta)+(y-\beta(s))\sin(\theta))^2\right)}{r_2^6}\right]\\
&-\mathrm{sgn}\left((y-\beta(s))\cos(\theta)-(x-\alpha(s))\sin(\theta)\right)\\
&\times\int_0^{\infty}(\kappa(\xi)-\kappa_\infty(\xi))\,\mathrm{e}^{-\xi|(y-\beta(s))\cos(\theta)-(x-\alpha(s))\sin(\theta)|}\\
&\cos\left(((x-\alpha(s))\cos(\theta)+(y-\beta(s))\sin(\theta))\,\xi\right)\mathrm{d}\xi\Bigg\}\,\mathrm{d}s,
\end{aligned}$$

$$\begin{aligned}
\sigma_{Yz} = \frac{G}{2\pi}\int_{-1}^{1} b_z(s)\sqrt{\left[\alpha'(s)\right]^2+\left[\beta'(s)\right]^2}\times\Bigg\{&\left(\left(\frac{L'}{2L}\right)^2-1\right)\frac{(x-\alpha(s))\cos(\theta)+(y-\beta(s))\sin(\theta)}{r_2^2}\\
&-L'\mathrm{sgn}\left((y-\beta(s))\cos(\theta)-(x-\alpha(s))\sin(\theta)\right)\\
&\times\frac{|(y-\beta(s))\cos(\theta)-(x-\alpha(s))\sin(\theta)|\,((x-\alpha(s))\cos(\theta)+(y-\beta(s))\sin(\theta))}{r_2^4}\\
&+\left[2L^2((x-\alpha(s))\cos(\theta)+(y-\beta(s))\sin(\theta))\right]\\
&\times\frac{\left(((x-\alpha(s))\cos(\theta)+(y-\beta(s))\sin(\theta))^2-3((y-\beta(s))\cos(\theta)-(x-\alpha(s))\sin(\theta))^2\right)}{r_2^6}
\end{aligned}$$

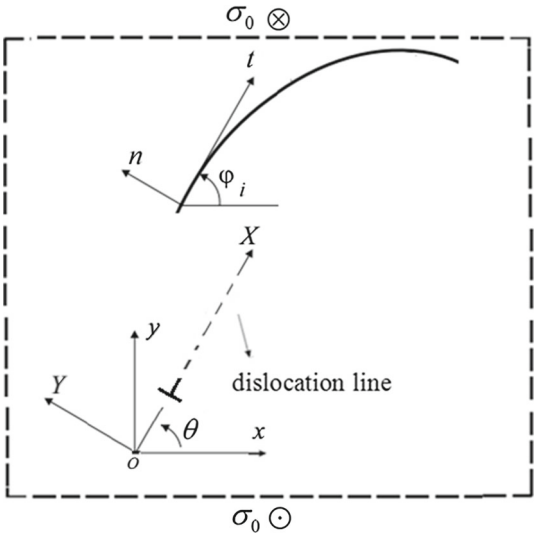

Fig. 3 Schematic view of the plane with a curved crack

$$+\int_0^{\infty}(\kappa(\xi)-\kappa_{\infty}(\xi))\,\mathrm{e}^{-\xi|(y-\beta(s))\cos(\theta)-(x-\alpha(s))\sin(\theta)|}\sin(((x-\alpha(s))\cos(\theta)$$
$$+(y-\beta(s))\sin(\theta))\,\xi)\,\mathrm{d}\xi\}\;\mathrm{d}s. \tag{25}$$

Note that Eq. (25) is the local stress in θ angle. The stresses in the local (X,Y) axis (Eq. 25) are identical with those in the global (x, y) set given in (22) at $\theta = 0$.

It is worth emphasizing that in Eq. (25), a prime denotes differentiation with respect to the arguments, the and $r_2^2 = ((x-\alpha(s))\cos(\theta)+(y-\beta(s))\sin(\theta))^2+((y-\beta(s))\cos(\theta)-(x-\alpha(s))\sin(\theta))^2$. If N is the number of cracks in the plane, Fig. (3), the curved crack configuration with respect to the coordinate system x, y may be described in a parametric form as:

$$x_i=\alpha_i(q),\ y_i=\beta_i(q),\quad i=1,2,\ldots,N,\quad -1\le q\le 1. \tag{26}$$

In the above relation, q is a parameter so that the coordinate of a crack configuration may be described based in parametric form.

The moveable orthogonal t, n local coordinate system is chosen in a way so that the origin may move on the crack, while the t-axis remains tangent to the crack surface [56].

The anti-plane traction on the surface of the i-th crack in terms of the stress components in the local Cartesian coordinates becomes:

$$\sigma_{nz}(x_i, y_i)=\sigma_{Yz}\cos(\psi_i)-\sigma_{Xz}\sin(\psi_i) \tag{27}$$

where $\theta=\phi_j$ is the angle between the axis of the local coordinate axes (X) relative to the x axis coordinate and $\varphi_i(q)=\tan^{-1}(\beta_i'(q)/\alpha_i'(q))$ is the angle between x and the moveable orthogonal t axis, also $\psi_i=\phi_i-\phi_j$. Equation (27) means that the local stress σ_{nz} is related to the local stresses σ_{Yz}, σ_{Xz} by the elementary stress transformation [57]. Suppose that the screw dislocation with unknown densities $B_{zj}(s)$ is distributed on the infinitesimal segment $\sqrt{[\alpha_j'(s)]^2+[\beta_j'(s)]^2}\mathrm{d}s$ at the surface of the j-th crack where the parameter $-1\le s\le 1$. The anti-plane traction on the surface of the i-th crack in the plane due to the presence of the above-mentioned distribution of dislocations on all N cracks yields:

$$\sigma_{nz}(\alpha_i(q),\beta_i(q))=\sum_{j=1}^{N}\int_{-1}^{1}K_{ij}(q,s)B_{zj}(s)\mathrm{d}s,\quad -1\le q\le 1,\quad i=1,2,\ldots,N. \tag{28}$$

Incorporating the crack angle $\psi_i(q)$, as seen in Fig. 3, into Eq. (28), the kernel is recast in a more convenient form as:

$$K_{ij}(q,s) = \begin{cases} -k^1_{xz}(\alpha_i,\beta_i,\alpha_j,\beta_j)\sin\psi_i + k^1_{yz}(\alpha_i,\beta_i,\alpha_j,\beta_j)\cos\psi_i, \left(\alpha_i(q)-\alpha_j(s)\right)\sin(\theta) \le \left(\beta_i(q)-\beta_j(s)\right)\cos(\theta) \\ -k^2_{xz}(\alpha_i,\beta_i,\alpha_j,\beta_j)\sin\psi_i + k^2_{yz}(\alpha_i,\beta_i,\alpha_j,\beta_j)\cos\psi_i, \left(\beta_i(q)-\beta_j(s)\right)\cos(\theta) < \left(\alpha_i(q)-\alpha_j(s)\right)\sin(\theta) \end{cases}. \tag{29}$$

The functions $k^h_{jz}(\alpha_i,\beta_i,\alpha_j,\beta_j)$, $h=1,2$, $j=x,y$ are introduced in (24). We should point out that in (29) quantities with subscript i are functions of q, whereas those with subscript j are functions of s. Drawing on the Buckner's principal [57,58], the elasticity problem of a plane in the absence of cracks under external loading should be solved which yields the traction on the crack surfaces with the opposite sign. Therefore, the left-hand side of Eq. (28), with the opposite sign, is the traction caused by external loading in the infinite plane without cracks on the presumed surfaces of cracks and may be distinct from Eq. (28). The applied tractions at the far-field σ_0 are considered to be uniform, and the kernel of integral (28) becomes:

$$\begin{aligned}
K^1_{ij}(q,s) = {} & \frac{G}{2\pi}\sqrt{\left[\alpha'_j(s)\right]^2+\left[\beta'_j(s)\right]^2} \\
& \times\Bigg\{\Bigg[\left(\left(\frac{L'}{2L}\right)^2-1\right)\frac{\chi}{R^2} - L'\frac{\vartheta\chi}{R^4} + \frac{2L^2\chi}{R^6}\left(\chi^2-3\vartheta^2\right) \\
& + \int_0^\infty \left(\kappa(\xi)-\kappa_\infty(\xi)\right)e^{-\xi\vartheta}\sin(\chi\xi)d\xi\Bigg]\cos\psi_i(q) \\
& - \Bigg[\left(1-\left(\frac{L'}{2L}\right)^2\right)\frac{\vartheta}{R^2} + \frac{L'}{2}\frac{\vartheta^2-\chi^2}{R^4} + \frac{2L^2\vartheta}{R^6}\left(\vartheta^2-3\chi^2\right) \\
& - \int_0^\infty \left(\kappa(\xi)-\kappa_\infty(\xi)\right)\mathrm{e}^{-\xi\vartheta}\cos(\chi\xi)\mathrm{d}\xi\Bigg]\sin\psi_i(q)\Bigg\},\ \vartheta\ge 0, \\
K^2_{ij}(q,s) = {} & \frac{G}{2\pi}\sqrt{\left[\alpha'_j(s)\right]^2+\left[\beta'_j(s)\right]^2} \\
& \times\Bigg\{\Bigg[\left(\left(\frac{L'}{2L}\right)^2-1\right)\frac{\chi}{R^2} + L'\frac{\vartheta\chi}{R^4} + \frac{2L^2\chi}{R^6}\left(\chi^2-3\vartheta^2\right) \\
& + \int_0^\infty \left(\kappa(\xi)-\kappa_\infty(\xi)\right)e^{\xi\vartheta}\sin(\chi\xi)d\xi\Bigg]\cos\psi_i(q) \\
& - \Bigg[\left(1-\left(\frac{L'}{2L}\right)^2\right)\frac{\vartheta}{R^2} - \frac{L'}{2}\frac{\vartheta^2-\chi^2}{R^4} + \frac{2L^2\vartheta}{R^6}\left(\vartheta^2-3\chi^2\right) \\
& + \int_0^\infty \left(\kappa(\xi)-\kappa_\infty(\xi)\right)e^{\xi\vartheta}\cos(\chi\xi)\mathrm{d}\xi\Bigg]\sin\psi_i(q)\Bigg\},\ \vartheta<0
\end{aligned} \tag{30}$$

in which $\chi = \left(\alpha_i(q)-\alpha_j(s)\right)\cos(\theta) + \left(\beta_i(q)-\beta_j(s)\right)\sin(\theta)$, $\vartheta = \left(\beta_i(q)-\beta_j(s)\right)\cos(\theta) - \left(\alpha_i(q)-\alpha_j(s)\right)\sin(\theta)$. It should be noted that in the absence of length effect parameters the obtained equations of strain gradient theory are turned into the same equations presented in the classic mechanics. The kernels of Eq. (28) are singular as $R\to 0$, or for $i=j$ as $q\to s$ and $R^2=\chi^2+\vartheta^2$. To extract the hypersingular

terms, the Taylor series expansion of $\alpha_j(s)$ and $\beta_j(s)$ in the vicinity of the points q is plugged into Eq. (30) yielding [56]:

$$K_{jj}(q,s)=\begin{cases}\frac{a^1_{-3j}(q)}{(s-q)^3}+\frac{a^1_{-2j}(q)}{(s-q)^2}+\frac{a^1_{-1j}(q)}{(s-q)}+\sum\limits_{m=0}^{\infty}a^1_{mj}(s-q)^m, & \vartheta\geq 0\\ \frac{a^2_{-3j}(q)}{(s-q)^3}+\frac{a^2_{-2j}(q)}{(s-q)^2}+\frac{a^2_{-1j}(q)}{(s-q)}+\sum\limits_{m=0}^{\infty}a^2_{mj}(s-q)^m, & \vartheta<0.\end{cases} \tag{31}$$

All of the coefficients of singular and hypersingular terms (a^p_{-nj}, $p=1,2$, $n=1,2,3$) are addressed in "Appendix B".

The series in (31) are regular, and the coefficients of the regular terms (a^p_{mj}, $p=1,2$, $m=1,2,\ldots$) are functions of variable q in the interval $-1\leq q\leq 1$, which do not take part in the ensuing analysis and are also too lengthy to be presented here.

As was discussed previously, the dominant singularity of stress fields for a dislocation as $R\to 0$ is of hypersingularity type. Consequently, Eq. (28) is a hypersingular integral equation for the dislocation densities. Employing the definition of dislocation density function, the equation for the crack opening displacement across the j-th crack becomes:

$$w_j^-(q)-w_j^+(q)=\int_{-1}^{q}\sqrt{[\alpha_j'(s)]^2+[\beta_j'(s)]^2}B_{zj}(s)\mathrm{d}s,\quad j=1,2,\ldots,N. \tag{32}$$

The displacement field is single-valued out of the crack the surfaces. Thus, the dislocation densities are subjected to the following closure requirements:

$$\int_{-1}^{1}\sqrt{[\alpha_j'(s)]^2+[\beta_j'(s)]^2}B_{zj}(s)\mathrm{d}s,\quad j=1,2,\ldots,N. \tag{33}$$

To obtain the dislocation density, the integral equations (28) and (33) are to be solved simultaneously. This is accomplished by means of Gauss–Chebyshev quadrature scheme developed in Erdogan et al. [59]. The stress fields exhibit hypersingularity at the crack tips; therefore, the dislocation densities are taken in the following forms [39]:

$$\begin{aligned}B^{SGT}_{zj}(s)&=\sqrt{1-s^2}\sum_{n=0}^{M}A^j_nU_n(s),\ U_n(s)\\&=\frac{\sin[(n+1)\cos^{-1}(s)]}{\sin[\cos^{-1}(s)]},\ -1\leq s\leq 1,\quad j=1,2,\ldots,N,\quad n=0,1,2,\ldots\end{aligned} \tag{34}$$

In relation (34) $U_n(s)$ is the Chebyshev polynomial of the second kind. In order to circumvent the difficulties which may be encountered in the numerical solution of the hypersingular integral Eq.(28) for cracks, we substitute (34) with (33). Formally, the integration with the closure requirement, i.e., $w_j^-(1)-w_j^+(1)=0$, leads to the following equation [39]:

$$\int_{-1}^{1}\sqrt{1-s^2}\sum_{n=0}^{M}A^j_nU_n(s)\,\mathrm{d}s=\begin{cases}\frac{\pi}{2}A^j_0 & \text{for } n=0\\ 0 & \text{for } n\neq 0.\end{cases} \tag{35}$$

According to the behavior of function $U_n(s)$, Eq. (33) is satisfied, when it requires the relation $A^j_0=0$ (see Eq. 35). The hypersingular parts of the kernels in the integral equation (28) should be separated from the regular part. Eq. (28), in light of (31), and may be rewritten as:

$$\begin{aligned}&\sigma_{nz}(\alpha_i(q),\beta_i(q))\\&=\sum_{n=1}^{M}\int_1^1\left\{A^i_n\left[\frac{a_{-3i^k}(q)}{(s-q)^3}+\frac{a^k_{-2i}(q)}{(s-q)^2}+\frac{a^k_{-1i}(q)}{(s-q)}+\left(K_{ii}(q,s)-\frac{a^k_{-3i}(q)}{(s-q)^3}-\frac{a^k_{-2i}(q)}{(s-q)^2}-\frac{a^k_{-1i}(q)}{(s-q)}\right)\right]\right.\end{aligned}$$

$$+\sum_{\substack{j=1\\ j\neq i}}^{N} A_n^j K_{ij}(q,s)\Bigg\} U_n(s)\sqrt{1-s^2}\mathrm{d}s, \quad -1\le q\le 1, \quad i=1,2,3,\ldots,N, \quad k=1,2. \tag{36}$$

It is worth mentioning that in the right-hand sides of Eq. (36) the first two terms are hypersingular. The next term is Cauchy singular, and the remaining terms are regular in the domain of integration.

3.1 Solution of the integral equations

Substitution of (31), (B.1–B.3) with the relevant terms of Eq. (36), in conjunction with the application of the following integration formulas [42]:

$$\int_{-1}^{1}\frac{U_n(s)\sqrt{1-s^2}}{s-q}\mathrm{d}s=\frac{\pi}{2}\left[U_{n-1}(q)-U_{n+1}(q)\right], \int_{-1}^{1}\frac{U_n(s)\sqrt{1-s^2}}{(s-q)^2}\mathrm{d}s=-\pi(n+1)U_n(q) \quad \text{for } n=0,$$

$$\int_{-1}^{1}\frac{U_n(s)\sqrt{1-s^2}}{(s-q)^3}\mathrm{d}s=\begin{cases}\pi\\ \frac{\pi}{4(1-q^2)}\left[-\left(n^2+3n+2\right)U_{n-1}(q)+\left(n^2+n\right)U_{n+1}(q)\right]\end{cases} \text{for } 1\le n \tag{37}$$

modifies Eq. (36) as:

$$\sigma_{nz}(\alpha_i(q),\beta_i(q))=\sum_{n=1}^{M}\left(A_n^i F_n(q)+\sum_{\substack{j=1\\ i\neq j}}^{N} A_n^j G_{nij}(q)\right), \quad -1\le q\le 1, \quad i=1,2,3,\ldots,N \tag{38}$$

and

$$\begin{aligned}F_n(q)=&\frac{\pi a_{-3i}^k(q)}{4\left(1-q^2\right)}\left[-\left(n^2+3n+2\right)U_{n-1}(q)+\left(n^2+n\right)U_{n+1}(q)\right]-a_{-2i}^k(q)\pi(n+1)U_n(q)\\ &+\frac{\pi a_{-1i}^k(q)}{2}\left[U_{n-1}(q)-U_{n+1}(q)\right]\\ &+\int_{-1}^{1}\left(K_{ii}(q,s)-\frac{a_{-3i}^k(q)}{(s-q)^3}-\frac{a_{-2i}^k(q)}{(s-q)^2}-\frac{a_{-1i}^k(q)}{(s-q)}\right)U_n(s)\sqrt{1-s^2}\mathrm{d}s,\\ G_{nij}(q)=&\int_{-1}^{1}K_{ij}(q,s)U_n(s)\sqrt{1-s^2}\mathrm{d}s, k=1,2.\end{aligned} \tag{39}$$

The unknown coefficients (A_n^j) for cracks are determined by solving the system of algebraic Eq. (38). The integral in Eq. (38) is calculated by Gauss–Chebychev and Gauss–Kronrod quadrature rules [60]. For the sake of numerical expediency, the collocation points q_i for discretizing the domain, $-1\le q\le 1$, in Eq. (38), and for the coefficients of the integral density of dislocation as s_k are chosen in the middle of Gauss–Chebychev quadrature points, and the integral equations reduced to the following system of $t\times M$ algebraic equations, where the collocation point (integration point) is presented below [60]:

$$q_i=\cos\left(\frac{(2i-1)\pi}{2(t+1)}\right) \quad i=1,2,\ldots,t-1. \tag{40}$$

Taking $t>M+1$, the resultant over-determined system of equations should be solved in terms of least-squares minimization. The number of terms in series, the number of collocation points on cracks, and interaction with

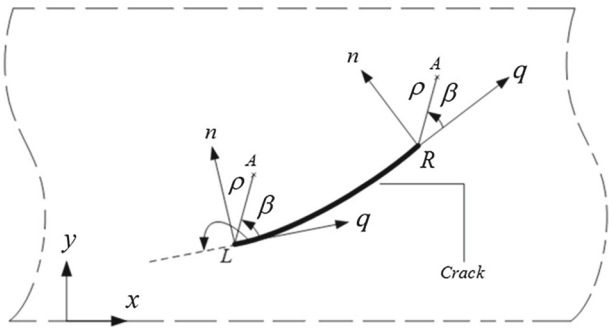

Fig. 4 Schematic view of a crack in polar coordinates to calculate the SIF

them are different. Nonetheless, a sufficient number of collocation points should be taken on a crack to ensure the convergence of the coefficients of the series. Considering the examples solved in this study, we realized that accurate results may be obtained by taking the number of collocation points about 1.2 times higher than the number of series terms.

3.2 Calculation of the stress intensity factor

In order to investigate the stress hypersingularity near the crack tip, we need to obtain stress expressions for our problem. We recognized that while the stresses inside the crack give us the system of hypersingular integral equations, these equations also provide us with the stress expressions outside the crack at the q axis (Fig. 4), provided the density functions are known [61].

In Fig. 4 the movable orthogonal coordinate system $n-q$ is chosen on the ith crack such that the origin locates on the crack, while the q-axis remains tangent to the crack surface.

By using the following relation (41), Eq. (36) can be stated as Eq. (42) [39]:

$$\int_{-1}^{1}\frac{U_n(s)\sqrt{1-s^2}}{(s-q)^3}=\frac{-\pi}{2}(n+1)\left(q-\frac{|q|}{q}\sqrt{q^2-1}\right)^{n-1}\left[n\left(1-\frac{|q|}{\sqrt{q^2-1}}\right)^2+\frac{q-\frac{|q|}{q}\sqrt{q^2-1}}{\sqrt{q^2-1}^3}\right],\ |q|>1,$$

$$\int_{-1}^{1}\frac{U_n(s)\sqrt{1-s^2}}{(s-q)^2}\mathrm{d}s=-\pi(n+1)\left(1-\frac{|q|}{\sqrt{q^2-1}}\right)\left(q-\frac{|q|}{q}\sqrt{q^2-1}\right)^{n},\ |q|>1,$$

$$\int_{-1}^{1}\frac{U_n(s)\sqrt{1-s^2}}{(s-q)}\mathrm{d}s=-\pi\left(q-\frac{|q|}{q}\sqrt{q^2-1}\right)^{n+1},\ |q|>1, \tag{41}$$

$$\begin{aligned}&\sigma_{nz}(\alpha_i(q),\beta_i(q))\\&=\sum_{n=1}^{M}A_n^i\left\{\frac{-\pi a_{-3i}^k(q)}{2}(n+1)\left(q-\frac{|q|}{q}\sqrt{q^2-1}\right)^{n-1}\left[n\left(1-\frac{|q|}{\sqrt{q^2-1}}\right)^2+\frac{q-\frac{|q|}{q}\sqrt{q^2-1}}{\sqrt{q^2-1}^3}\right]\right.\\&-\pi a_{-2i}^k(q)(n+1)\left(1-\frac{|q|}{\sqrt{q^2-1}}\right)\left(q-\frac{|q|}{q}\sqrt{q^2-1}\right)^{n}-\pi a_{-1i}^k(q)\left(q-\frac{|q|}{q}\sqrt{q^2-1}\right)^{n+1}\\&\left.+\int_{-1}^{1}\left[K_{ii}(q,s)-\frac{a_{-3i}^k(q)}{(s-q)^3}-\frac{a_{-2i}^k(q)}{(s-q)^2}-\frac{a_{-1i}^k(q)}{(s-q)}\right]U_n(s)\sqrt{1-s^2}\mathrm{d}s\right\}\\&+\sum_{\substack{j=1\\j\neq i}}^{N}\int_{-1}^{1}K_{ij}(q,s)\sum_{n=1}^{M}A_n^jU_n(s)\sqrt{1-s^2}\mathrm{d}s,\qquad |q|>1,\quad i=1,2,3,\ldots,N,\ \ k=1,2.\end{aligned} \tag{42}$$

The SIFs in the strain gradient are calculated as [39]:

$$L(K_{\mathrm{III}})_{Ri}=\lim_{\rho\to0}2\rho\sqrt{2\pi\rho}\sigma_{nz}(\rho,0),\quad L(K_{\mathrm{III}})_{Li}=\lim_{\rho\to0}2\rho\sqrt{2\pi\rho}\sigma_{nz}(\rho,\pi). \tag{43}$$

We expect the stresses to be hypersingular at the crack tips. Furthermore, from Eq. (41), we infer that any singular terms in the stresses weaker than the square and cubic root singularity, as well as regular terms, will vanish because of the expressions in the limiting process. Also considering that the terms involving kernels are bounded everywhere, the limiting process will serve to eliminate them, and we just need to concern ourselves with the hypersingular terms. We may express the leading terms of shear stress at the beginning of the crack tip. So, in the evaluation of SIF, only the hypersingular term of stress is considered. By substituting the hypersingular term of (41) with (43), it leads to:

$$\begin{aligned} L\left(K_{\mathrm{III}}\right)_{Ri}^{SGT} &= \frac{-1}{2}\pi^{\frac{3}{2}}\Gamma\left(1\right)^{\frac{3}{4}}\left[a_{-3i}\left(1\right)\sum_{n=1}^{M}A_n^i\left(n+1\right)\right], \\ L\left(K_{\mathrm{III}}\right)_{Li}^{SGT} &= \frac{1}{2}\pi^{\frac{3}{2}}\Gamma\left(-1\right)^{\frac{3}{4}}\left[a_{-3i}\left(-1\right)\sum_{n=1}^{M}A_n^i\left(-1\right)^n\left(n+1\right)\right] \end{aligned} \tag{44}$$

where $\Gamma\left(q\right)=\left(\alpha_j'\left(q\right)\right)^2+\left(\beta_j'\left(q\right)\right)^2$. In the above calculation, we use [61]:

$$\begin{aligned} \rho_{Ri} &= \sqrt{\left(\left(\alpha_i\left(q\right)-\alpha_j\left(1\right)\right)\right)^2+\left(\left(\beta_i\left(q\right)-\beta_j\left(1\right)\right)\right)^2}\approx\Gamma\left(1\right)^{\frac{1}{2}}\left(q-1\right),\ q\to 1, \\ \rho_{Li} &= \sqrt{\left(\left(\alpha_i\left(q\right)-\alpha_j\left(-1\right)\right)\right)^2+\left(\left(\beta_i\left(q\right)-\beta_j\left(-1\right)\right)\right)^2}\approx\Gamma\left(-1\right)^{\frac{1}{2}}\left(q+1\right),\ q\to -1. \end{aligned} \tag{45}$$

The stress intensity factors for cracks in the vicinity of crack tips in terms of the density of dislocation coefficient, A_n^i, in strain gradient theory are given in Eq. (46):

$$\begin{aligned} L\left(K_{\mathrm{III}}\right)_{Ri}^{SGT} &= \frac{-G\sqrt{\pi}}{4}\sum_{n=1}^{M}A_n^i\left(n+1\right)\Gamma\left(1\right)^{\frac{3}{4}} \\ &\times\left\{\frac{2L^2\cos\psi_i\left(1\right)}{\Gamma\left(1\right)^{\frac{5}{2}}}\left(\eta\left(1\right)^3-3\eta\left(1\right)\varepsilon\left(1\right)^2\right)-\frac{2L^2\sin\psi_i\left(1\right)}{\Gamma\left(1\right)^{\frac{5}{2}}}\left(\varepsilon\left(1\right)^3-3\varepsilon\left(1\right)\eta\left(1\right)^2\right)\right\}, \\ L\left(K_{\mathrm{III}}\right)_{Li}^{SGT} &= \frac{G\sqrt{\pi}}{4}\sum_{n=1}^{M}A_n^i\left(-1\right)^n\left(n+1\right)\Gamma\left(-1\right)^{\frac{3}{4}} \\ &\times\left\{\frac{2L^2\cos\psi_i\left(-1\right)}{\Gamma\left(-1\right)^{\frac{5}{2}}}\left(\eta\left(-1\right)^3-3\eta\left(-1\right)\varepsilon\left(-1\right)^2\right)-\frac{2L^2\sin\psi_i\left(-1\right)}{\Gamma\left(-1\right)^{\frac{5}{2}}}\left(\varepsilon\left(-1\right)^3-3\varepsilon\left(-1\right)\eta\left(-1\right)^2\right)\right\}. \end{aligned} \tag{46}$$

In the above equation $\eta\left(q\right)=-\alpha_j'\left(q\right)\cos\left(\theta\right)-\beta_j'\left(q\right)\sin\left(\theta\right)$, $\varepsilon\left(q\right)=-\beta_j'\left(q\right)\cos\left(\theta\right)+\alpha_j'\left(q\right)\sin\left(\theta\right)$. For each crack, since the difference between angle(φ_j) and (φ_i) is zero, the above equations are reformed by replacing $\psi_j\left(-1\right)=\psi_j\left(1\right)=0$, also after some elaborations on trigonometric relations, the final forms of stress intensity factors are obtained as follows:

$$\begin{aligned} \left(K_{\mathrm{III}}\right)_{Ri}^{SGT} &= \frac{GL\sqrt{\pi}}{2}\Gamma\left(1\right)^{\frac{-1}{4}}\sum_{n=1}^{M}A_n^i\left(n+1\right), \\ \left(K_{\mathrm{III}}\right)_{Li}^{SGT} &= \frac{-GL\sqrt{\pi}}{2}\Gamma\left(-1\right)^{\frac{-1}{4}}\sum_{n=1}^{M}A_n^i\left(-1\right)^n\left(n+1\right). \end{aligned} \tag{47}$$

In relation (47) the subscripts L and R designate the left and the right crack tips, respectively. The solutions of Eq. (38) are plugged into (47) to calculate the stress intensity factors for strain gradient theory. In Eq.(47), the dimensionless quantities and the new variable $\tilde{L}=L/a$ and $\tilde{L}'=L'/a$ can be utilized.

Table 1 Comparison of the non-dimensional SIF for different dimensionless parameters $\tilde{L}$, $\tilde{L}'$

Size effect	[39]	[42]	[46]	Present work	Error%
$\tilde{L} = 0.2$ $\tilde{L}' = 0.04$		0.87921		0.8803	0.1239
$\tilde{L} = 0.05$ $\tilde{L}' = 0.01$		0.97113		0.9722	0.110
$\tilde{L} = 0.1$ $\tilde{L}' = 0.01$			0.9438	0.9377	0.650
$\tilde{L} = 0.05$ $\tilde{L}' = 0.005$			0.9720	0.9687	0.340
$\tilde{L} = 0.025$ $\tilde{L}' = 0.0025$			0.9863	0.9789	0.750
$\tilde{L} = 0.8$ $\tilde{L}' = 0$	0.5280			0.5280	0
$\tilde{L} = 0.5$ $\tilde{L}' = 0$	0.6978			0.6978	0
$\tilde{L} = 0.2$ $\tilde{L}' = 0$	0.8934			0.8934	0
$\tilde{L} = 0.1$ $\tilde{L}' = 0$	0.9486			0.9486	0
$\tilde{L} = 0.05$ $\tilde{L}' = 0$	0.9747			0.9747	0

4 Results and discussion

In this Section, some examples are demonstrated to show the ability and the accuracy of the distributed dislocation technique. In the first three examples, the quantity for making the stress intensity factors dimensionless is $k_0 = \sigma_0\sqrt{\pi a}$ where a is the half length of a straight crack and all lengths are dimensionless by the half length of the straight crack. Also, the plane is considered under uniform traction in far field σ_0. The first example is for the validation of results, and the others are new problems considered for the first time in the framework of strain gradient theory.

4.1 Comparison with literature

In order to verify the distributed dislocation solution, stress intensity factors of the infinite plane are determined. Indeed, this value is directly related to the stress intensity factor as it is predicted by the integral solution method [39,42,46]. The percentage of the error of the distributed dislocation solution was calculated using the comparison between the stress intensity factor predicted via the present work and those in the literature (integral solution), which is reported in Table 1.

As seen, for the first case in Table 1, one can achieve less than 2% error which is in an excellent range for most engineering applications.

Also, as it is shown, both internal length ($\tilde{L}$) and director length ($\tilde{L}'$) have an effect on the SIF and may be significant. However, the effects of these internal lengths can be negligible beyond the nano-scale. The function of the internal length $\tilde{L}$ is to cover the applied tractions leading to crack stiffening, and the function of the director length $\tilde{L}'$ is to magnify the applied tractions leading to crack compliance by raising the energy relinquish rate of the crack.

Although $\tilde{L}$ and $\tilde{L}'$ have similar impacts (all are positive), i.e., the influence of variation of $\tilde{L}$ is similar to that of $\tilde{L}'$, the effect of the internal length on the SIF is more significant than that of the director length since the value of $\tilde{L}'$ does not appear in Eq (47). Furthermore, the director length $\tilde{L}'$ cannot exist alone (i.e. $\tilde{L} = 0$ and $\tilde{L}' \neq 0$ is not acceptable conformation) because the strain energy density function requires to be non-negative. Therefore, it will be quite adequate if we only study the effect of $\tilde{L}$ on the SIF. ($\tilde{L}'$ is not crucial, hence, it can be claimed that the inclusion of $\tilde{L}'$ is not necessary).

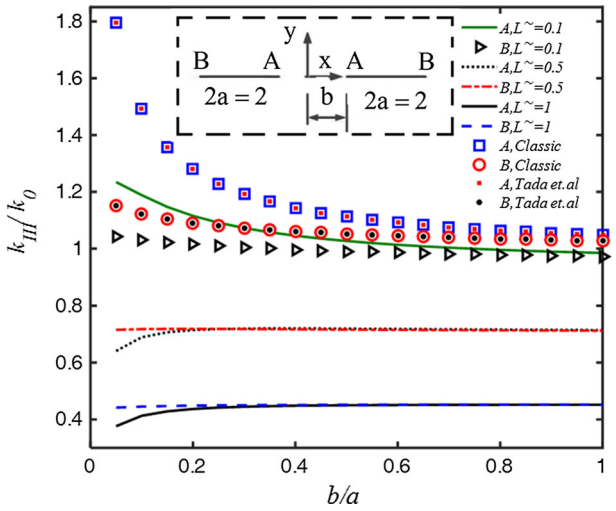

Fig. 5 Dimensionless mode III stress intensity factors for two collinear cracks ($\tilde{L}' = 0.9\tilde{L}$)

As was mentioned before, normalizing these internal lengths with the crack length was done by a new variable $\tilde{L} = L/a$ and $\tilde{L}' = L'/a$. In this study, the reasonable values of normalized internal lengths are to be considered. It must be noted that these values based on which the results were derived were qualitative. In other words, with changes in the internal lengths, only the values will change but the trends will not change. The only limitation of the values of normalized internal lengths is that $\left|\tilde{L}'/\tilde{L}\right| < 1, \quad \tilde{L} \neq 0.$

In the next Sections, some examples will be demonstrated using strain gradient theory, and the continuum classic theory along with size effect will be studied. It should be noted that at nano-scale distances both size effects ($\tilde{L}$) should be taken into account for the precise calculation of the stress intensity factor parameters of the nano-structures.

4.2 Two parallel collinear cracks

Let us consider an the infinite plane weakened by two collinear straight cracks of length $2a$, under anti-plane deformation, Fig. 5. This Figure depicts the dependence of the ratio SIF upon the ratio of the distance between cracks b/a for classic and strain gradient theory.

The interaction of two receding straight cracks is discussed. the crack parametric expression is $\alpha_R(q) = x_{oR} + a_R q = [q + 1 + b]\, a, \beta_R(q) = y_{oR} = 0\, in\, -1 \leq q \leq 1$ for the right crack and $\alpha_L(q) = [q - 1 - b]\, a, \beta_L(q) = 0$ for the left crack. An approximate stress intensity factor in linear elastic fracture mechanics can be obtained from Tada [62]. In classical theory, the SIF for the tip of cracks increases with a reduction in the value of b/a. However, in strain gradient k_{III}/k_0 for a high value $\tilde{L}$ slightly decreases by lowering the b/a ratio, but by decreasing size effect this trend is similar to what was observed in classic theory. In other words, the stress intensity factors have remarkable amounts around two adjacent tips of cracks, and generally for any b/a ratio, as the size effect increases, their values gradually decrease as it is demonstrated. This difference is the result of the size effect which induces rigidity in the governing equation of the strain gradient. On the other hand, a different trend is observed in the case of two parallel collinear cracks: Indeed, (for low b/a) the presence of the size effect might increase or decrease the stress intensity factor. According to this Figure, it is clear that the strain gradient theory generally is less predictable for the SIF as opposed to the classic continuum theory. The classic continuum for small half crack length about material length size ($\tilde{L} = 1$) in low b/a ($b/a = 0.05$) values, predicts the SIF values about 4.7 times higher for A tips of crack and about 2.6 times higher for B tips of crack as compared with strain gradient theory. A decrease in the $\tilde{L}$ value (increase in the crack length) results in the strain gradient theory becoming similar to the results of classic continuum theory. In other words, enhancing the crack length ($2a$) increases the stress intensity factor and lowers the size-effect parameter $\tilde{L}$.

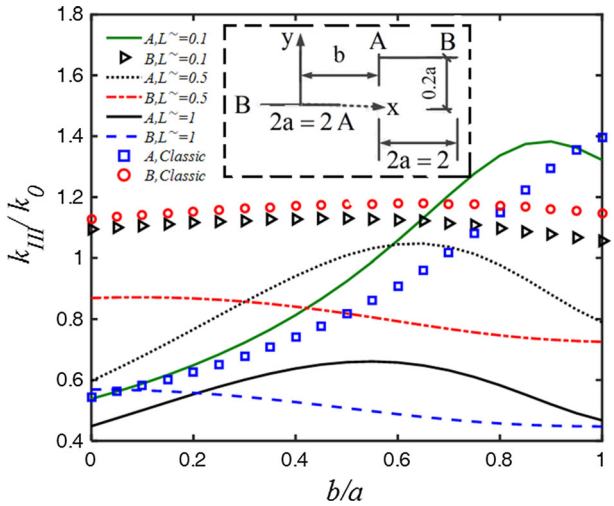

Fig. 6 Dimensionless mode III stress intensity factors for two parallel off-center cracks ($\tilde{L}' = 0.9\tilde{L}$)

All curves in the above Figure show that while strain gradient theory is the dominant factor for high values of $\tilde{L}$, the continuum classic theory is prominent in low $\tilde{L}$ values. Indeed, this trend is similar to what is predicted by classic theory [53–56].

As this Figure shows, when $\tilde{L}$ increases, the SIF decreases. The physical meaning of this phenomenon is that generally the size effect decreases the stress intensity factor, and it provides a hardening behavior that enhances the elastic resistance along with the consequent operation traction of the nano-structures. Another important result that we find out from this Figure is that large distances between tip cracks (big value of b/a) lead to a SIF which is regarded as a value product without interaction between the two cracks. For example, in classic theory when the distance between the cracks increases, the value of the SIF ratio curve reaches the value of 1, in case of a lonely crack, since the stress intensity factor for a crack in the classical continuum is 1.

4.3 Two parallel off-center cracks

Two off-center equal-length cracks which are parallel to the x axis are shown in Fig. 6. The left crack and the vertical distance between the cracks remain fixed, whereas the location of the right crack is changing in the direction of the x axis. The dimensionless stress intensity factors versus dimensionless location of the right crack are depicted in Fig. 6. Due to the symmetry, the SIFs at B and A of the left crack are equal to those at B and A of the right crack. In this case, the crack geometrical parametric expression is $\alpha_R(q) = [q + 1 + b]\,a$, $\beta_R(q) = 0.2a \; in \; -1 \le q \le 1$ for the right crack, and $\alpha_L(q) = aq$, $\beta_L(q) = 0$ for the left crack. Moreover, a considerable change in k_{III}/k_0 can be observed as b/a varies. The variation of the SIFs for B, tip crack, is much smaller than that of A, tip crack, due to the weak interaction between these tip cracks. Our results indicate that when $\tilde{L}$ tends to zero (increases the crack length), it means that the crack length is much larger than the characteristic length, the stress intensity factor tends continuously to its value of classical elasticity, and the impact of size effect vanishes. This trend is the same as that observed in Fig. 5, where the size effect decreases the stress intensity factor of the nano-structure. It means that the size effect provides a hardening behavior (decreases the stress intensity factor) in the elastic resistance of the nano-structure. The enhanced elastic resistance allowed the plane to tolerate higher values of applied traction before the fracture occurs, i.e., lower values of the stress intensity factor.

4.4 A fixed and a rotating crack

We consider two equal-length straight cracks situated on the plane, Fig. 7. Crack B_1A_1 is fixed while A_2B_2 with length $2a = 2$ is rotating around its center. The crack configurations in parametric form are:

$$\alpha_L(q) = -1.05 + aq, \quad \beta_L(q) = 0,$$

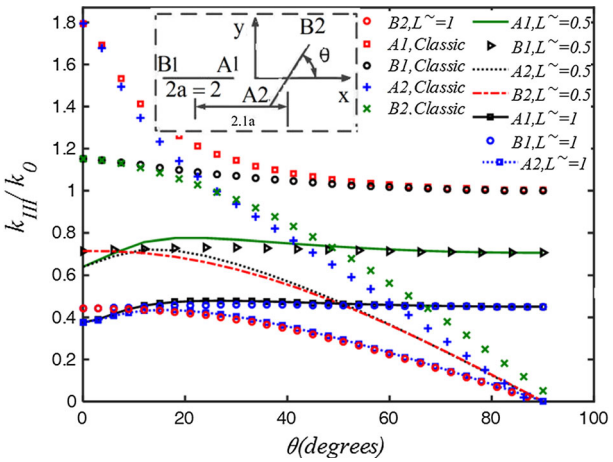

Fig. 7 Mode III stress intensity factors for a fixed and a rotating crack ($\tilde{L}' = 0.9\tilde{L}$)

$$\alpha_R(q) = 1.05 + aq\cos\theta, \quad \beta_R(q) = 1.05 + aq\sin\theta, \qquad -1 \le q \le 1 \tag{48}$$

where $a = 1$ is the half length of the cracks, and θ is the angle between crack A_2B_2 and the x-axis.

The variation of the dimensionless stress intensity factors versus the angle of rotation for classic theory, i.e., $\tilde{L}, \tilde{L}' = 0$ and gradient theory with $\tilde{L} = 0.5, 1$ and $\tilde{L}' = 0.9\tilde{L}$ is depicted in Fig. 7.

The variations of k_{III}^{B1} and k_{III}^{A1} are not significant and are due to the change in the interaction between the cracks.

In classical theory, the value of k_{III}^{A2} at small values of angle θ, $\theta < \pi/180$, is higher than k_{III}^{B2}, which is attributed to a stronger interaction with the fixed crack i.e., the distance between A_2 and A_1 is much shorter than that between B_2 and A_1. Interestingly, as seen in Fig. 7, this trend is different from what is observed in the case of strain gradient theory, where at small values of angle θ the value of k_{III}^{A2} is smaller than k_{III}^{B2}.

Another interesting trend observed in this Figure is that at larger values of angle θ in classical theory the interaction between the crack tip B_2 and the fixed crack enhances, also for A_2 and the fixed crack decreases, while in strain gradient theory at larger values of angle θ, $\left|k_{\mathrm{III}}^{A2}\right| > \left|k_{\mathrm{III}}^{B2}\right|$. In other words, in strain gradient theory for small distance between the tip cracks, the size effect is stronger than the interaction between tip cracks, and it has more severe effects on the stress intensity factor.

On the other hands, a different trend is observed in the case of strain gradient: Indeed, the amount of size effect might decrease (for high $\tilde{L}', \tilde{L}$) or increase (for low $\tilde{L}', \tilde{L}$) the SIF. This trend is similar to what is observed in Fig. 5.

At $\theta = \pi/2$, the applied traction on the crack surface A_2B_2 is zero. Therefore, the stress intensity factors are zero, but the interaction between cracks produces unequal values of the stress intensity factor at the crack tips. The foregoing inequality is valid everywhere, except in a narrow band around $\theta = \pi/2$, which reverses. The difference between the trends is the result of the presence of the size effect. The results of the present study show that the existence of this size effect is a crucial issue to precisely determine the SIF parameters of the nano-structures which should be included in theoretical models.

4.5 A curved and a straight crack

In this example, we consider a stationary curved crack and a growing straight crack with a fixed center, inset in Fig. 8. The parametric representations of straight and curved cracks are identified as follows [63]:

$$\begin{aligned} &\alpha_L(q) = -m + aq, \quad \beta_L(q) = n, \\ &\alpha_R(q) = m \times \cos\left(\frac{\pi}{4}(1-q)\right), \quad \beta_R(q) = n \times \sin\left(\frac{\pi}{4}(1-q)\right) \end{aligned} \tag{49}$$

where $m = 2, n = 1.5$. Figure 8 shows the variation of the dimensionless stress intensity factors versus the length of the straight crack in the plane. As it may be from observed from k_{III}/k_0, the two approaching crack tips change rapidly. In contrast, the variations of k_{III}/k_0 for crack tips B1 and B2, especially B2, are not that

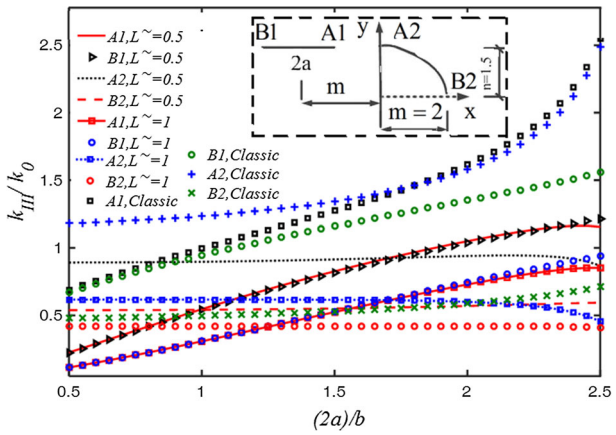

Fig. 8 Mode III stress intensity factors for a straight and a curved crack ($\tilde{L}' = 0.9\tilde{L}$)

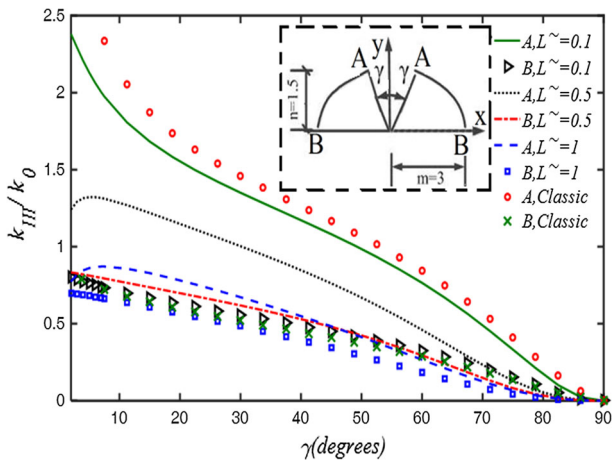

Fig. 9 Mode III stress intensity factors for two curved cracks ($\tilde{L}' = 0.9\tilde{L}$)

pronounced. The same results were obtained when two neighboring tip cracks approach each other, so that the trend in strain gradient and classic theory is different, which was discussed in the previous example.

4.6 Two curved cracks

In the last example two curved cracks, which are portions of the circumference of an ellipse with the following parametric representations, are considered:

$$\alpha_i(q) = x_c + (-1)^i m \cos\left[\frac{1}{2}\left(1-(-1)^i q\right)\tan^{-1}\left(\frac{m}{n}\cot\gamma\right)\right],$$
$$\beta_i(q) = y_c + n \sin\left[\frac{1}{2}\left(1-(-1)^i q\right)\tan^{-1}\left(\frac{m}{n}\cot\gamma\right)\right] - 1 \le q \le 1, \quad i = 1, 2. \tag{50}$$

The coordinates of the center of the ellipse are $(x_c, y_c) = (0, 0)$. The lengths of the major and the minor semi-axes of the ellipse are $m = 3$ and $n = 1.5$, respectively.

The problem is symmetric with respect to the y-axis. Thus, the stress intensity factors for crack tips are identical. The variation of the dimensionless stress intensity factors for three size effects $\tilde{L} = 0.1$, $\tilde{L} = 0.5$ and $\tilde{L} = 1$ as opposed to angle γ for the crack BA are shown in Fig. 9. The normalizing factor in this case is taken as $k_0 = \sigma_0\sqrt{\pi m}$. Nonetheless, the variation of the stress intensity factor for both theories manifests the same trend, except for the low distance between two adjacent tip cracks.

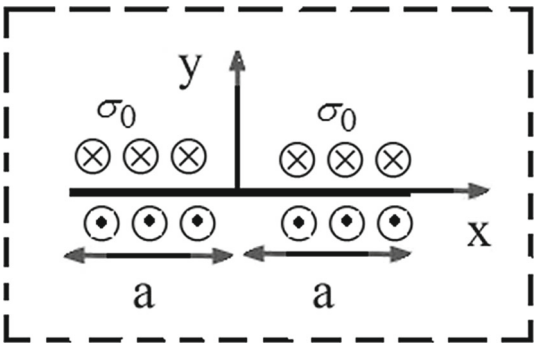

Fig. 10 Geometry of the medium with a horizontal crack

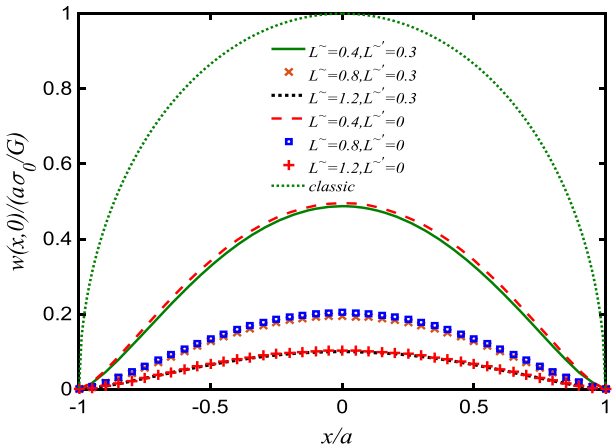

Fig. 11 Crack displacement profile for homogeneous material under uniform crack surface shear loading ($\sigma_0 = \sigma_{yz}$)

5 Case study of size effects on the crack opening displacement and stress and strain field

5.1 Crack opening displacement

Figure 10 shows a schematic representation of the medium with a horizontal crack. The normalized crack opening displacements for a homogeneous medium with the same strain gradient effect, shown in Fig. 11, is obtained by integrating the slope function (strain), according to Eq. (51). The crack profile in this Figure is symmetric due to the homogeneity of the material,

$$w\left(r,0\right)=a\int\limits_{-1}^{r}B_z\left(s\right)\mathrm{d}s=a\int\limits_{-1}^{r}\sqrt{1-s^2}\sum_{n=0}^{N}A_nU_n\left(s\right)\mathrm{d}s. \tag{51}$$

As shown in Fig. 11, the most well-known characteristic is the cusping phenomenon around the crack tips. In this Figure the main difference between curves relevant to classic and strain gradient theory is the cusp at the crack tips. As seen in this Figure, one may observe that the profile for classic theory has a tangent line with infinite slope at the crack tips, which is a usual crack behavior demonstrated in the classical LEFM. However, this is not the case in gradient theory as evidenced by the numerical results shown, and the profile at the crack tip has a small slope [64].

Also it can be concluded that the strain gradient theory predicts the crack opening displacement smaller than the classical theory [64].

It is emphasized that the cusping of the crack opening displacement at the crack tip by the gradient theory and the distributed dislocation technique were first pointed out in [51] and later discussed in [65,66].

The problem was addressed more recently [35], and references were quoted therein as well as in [67], where the distributed dislocation technique was employed by using the non-singular solutions for screw dislocations

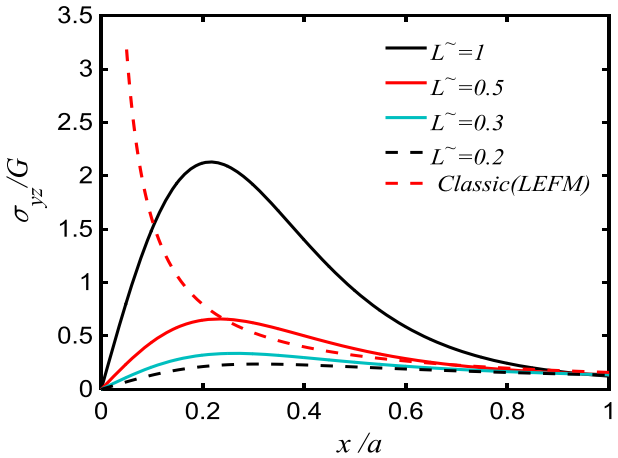

Fig. 12 Normalized stress distribution for a horizontal crack in a plane ($\tilde{L}' = 0.9\tilde{L}$)

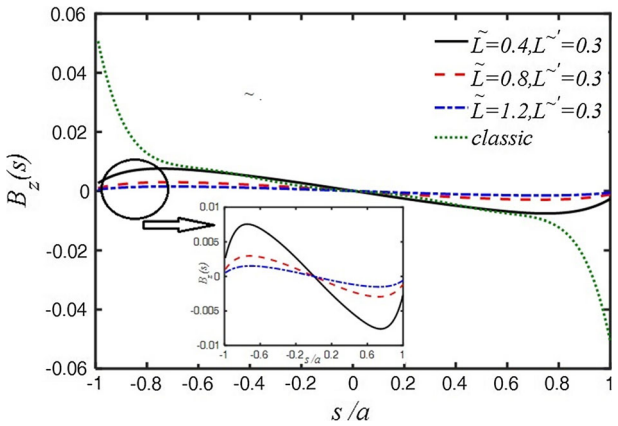

Fig. 13 Dislocation density for classical and strain gradient elasticity

derived, for example, in [37,38]. A most recent contribution along these lines [64] simply confirmed the earlier results indicating that the conventional gradient elasticity theory suffices, and no additional physical insight is gained by including extra higher order strain gradients.

5.2 Stress field

Figure 12 depicts the variation of shear stress (σ_{yz}) as a function of the length of the crack. As seen in Fig. 12, the stress highly increases and diverges in the classic LEFM as x approaches the crack tips along the ligament. Note that this trend is different from what is observed in strain gradient theory where the stress at the crack tip does not exhibit any jump behavior and has a finite amount.

5.3 Strain field

Figure 13 represent the influence of dislocation density of a crack the on the dimensionless length of the crack with considering size effects. Note that the dislocation density is in fact defined as the derivative of a displacement or ($B_z(s) = \frac{\partial w(s,0^+)}{\partial s}$). As seen, a decreasing size effect results in converging the strain profile to the slope function (strain) of the classical LEFM case in the region away from the crack tips; but at large size effect the strain is very different from its classical counterpart near the crack tips and has a singular trend. Moreover, the sign of the strain changes, as the size effect decreases the inner part i.e. the region away from of the two crack tips seems to converge to the solution of classical LEFM.

6 Conclusions

Stress analysis and simulation of a nano-crack subjected to anti-plane stresses are carried out in an infinite plane weakened by a screw dislocation. The solution is obtained in an integral form, which may be considered as the hypersingular integral for the plane with multiple cracks under anti-plane deformation. The new elastic constants, also referred to as characteristic lengths, become physically meaningful in the presence of structures and defects of comparable size. Thus, the stress intensity factor decreases, particularly near small defects which is a manifestation of the presence of a characteristic length. Comparing the numerical results shows that the distribution dislocation method works accurately in the framework of strain gradient elasticity and can be applied practically to the treatment of material discontinuities in ultra small scales. To study the interaction between cracks and also the effects of crack orientation, stress intensity factors are obtained for some examples, which are indicative of the capability of gradient elasticity theory to capture the size effect, which is quite considerable in nano-sized specimens. Also the ability of the distribution dislocation method will be considered.

Among other findings,

- We observed that the size effect becomes important for small sizes of nano-structures in a way that stress intensity factors will enhance as the size effect of the material decreases. Moreover, the size effect causes the plane with the assigned parameter to fail as a more rigid structure.
- As it was shown, the usual continuum theories are not capable of describing size effects because of neglecting the internal length scale parameter. They not only fail to provide such accurate results, but also their solutions often become deteriorated.
- Contribution of additional constants in the formulation of higher-order continuum theories or enhanced elasticity models, such as gradient theory, makes them capable of capturing the size effects quite adequately.
- Strain gradient modeling in addition to providing the accurate results, which are in good agreement with those obtained from the atomistic method, is such a powerful approach that is computationally less expensive than other approaches.
- As the characteristic length of the deformation field becomes significantly larger than the material length scale parameter, the strain gradients effect becomes negligible because the strain terms are much larger than their scaled gradient terms. In this case, the results obtained via strain gradient theory are the same as those of the classic theory.
- Since the geometrical characteristics of nano-structures are often of the order of several nanometers, the presence of material constants can influence nano-structures' treatment significantly.
- It can be concluded that in the nano-scale structures applying proper theories and analyzing them allows manufacturers to design and make more accurate devices; since in the case of using classic continuum theory, it will lead to an apparent error.

Appendix A: Physical meaning and implications of non-classical theory

All the following experiments imply that when the characteristic size (thickness, diameter, etc.) of a micro-/nano-element is of the order of its intrinsic material length scales (typically sub-micron), the material elastic constants highly depend on the element dimensions. The size-dependent behavior of materials and structures at sub-micron distances cannot be modeled using classical continuum mechanics.

It has been shown that torsional hardening of a copper wire increases by a factor of 3 as the wire diameter decreases from 170 to 12 μm [68]. Stolken and Evans [69] showed that a decrease in the thickness of thin nickel beams from 50 to 12.5 μm can lead to great increase in the plastic work hardening of the constitutive material. Also, the size-dependent behavior has been detected in some kinds of polymers [70]. For hardness measurement of bulk gold, it is found that the plastic length scale parameter (for indentation test and hardness behavior) of Au increases from 470 nm to 1.05 μm with increasing the Au film thickness from 500 nm to 2 μm [71]. Using micro-bend testing method, the plastic intrinsic material length scale of 4 μm for copper and 5 μm for nickel were determined [72].

Appendix B

The coefficients of the hypersingular terms in Eq. (31) are:

$$a^1_{-j}(q) = a^2_{-j}(q) = \frac{G}{2\pi\mu^{\frac{1}{2}}}\left(\left(\frac{L'}{2L}\right)^2 - 1\right)\left\{\Lambda\cos\psi_j(q) + \Omega\sin\psi_j(q)\right\}, \tag{B.1}$$

$$a^1_{-2j}(q) = -a^2_{-2j}(q) = -\frac{GL'}{2\pi\mu^{\frac{3}{2}}}\left\{\Omega\Lambda\cos\psi_j(q) + \frac{\Omega^2-\Lambda^2}{2}\sin\psi_j(q)\right\}, \tag{B.2}$$

$$a^1_{-3j}(q) = a^2_{-3j}(q) = \frac{GL^2}{\pi\mu^{\frac{5}{2}}}\left\{\left(\Lambda^3 - 3\Lambda\Omega^2\right)\cos\psi_j(q) - \left(\Omega^3 - 3\Omega\Lambda^2\right)\sin\psi_j(q)\right\} \tag{B.3}$$

where $\Lambda = -\alpha'_j(q)\cos(\theta) - \beta'_j(q)\sin(\theta)$, $\Omega = -\beta'_j(q)\cos(\theta) + \alpha'_j(q)\sin(\theta)$, $\mu = \left(\alpha'_j(q)\right)^2 + \left(\beta'_j(q)\right)^2$.

References

1. Broek, D.: Elementary Engineering Fracture Mechanics. Kluwer Academic Publishers, Southampton (1986)
2. Cosserat, E., Cosserat, F.: Theorie des Corps Deformables. dc.publisher Hermann et Fils, Paris (1909)
3. Toupin, R.A.: Elastic materials with couple stresses. Arch. Ration. Mech. Anal. **11**, 385–414 (1962)
4. Koiter, W.T.: Couple-stresses in the theory of elasticity: I and II. Proc. K. Ned. Akad. Wet. B **67**, 17–44 (1964)
5. Ozturk, M., Erdogan, F.: Antiplane shear crack problem in bonded materials with a graded interfacial zone. Int. J. Eng. Sci. **31**, 1641–1657 (1963)
6. Huang, G.Y., Wang, Y.S., Gross, D.: Fracture analysis of functionally graded coatings: antiplane deformation. Eur. J. Mech. A. Solids. **21**, 391–400 (2002)
7. Wang, B.L., Mai, Y.W., Sun, Y.G.: Anti-plane fracture of a functionally graded material strip. Eur. J. Mech. A. Solids. **22**, 357–368 (2003)
8. Wang, Y.S., Huang, G.Y., Gross, D.: On the mechanical modeling of functionally graded interfacial zone with a Griffith crack: anti-plane deformation. Trans. ASME J. Appl. Mech **70**, 676–680 (2003)
9. Fleck, N.A., Muller, G.M., Ashby, M.F., Hutchinson, J.W.: Strain gradient plasticity: theory and experiment. Acta Metall. Mater. **42**, 475–487 (1994)
10. Stolken, J.S., Evans, A.G.: A microbend test method for measuring the plasticity length scale. Acta Mater. **46**, 5109–5115 (1998)
11. Chong, A.C.M., Lam, D.C.C.: Strain gradient plasticity effect in indentation hardness of polymers. Int. J. Mater. Res. **14**, 4103–4110 (1999)
12. Mousavi, S.M., Paavola, J., Baroudi, D.: Distributed non-singular dislocation technique for cracks in strain gradient elasticity. J. Mech. Behav. Mater. **23**, 47–58 (2014)
13. Eringen, A.C., Edelen, D.B.G.: On nonlocal elasticity. Int. J. Eng. Sci. **10**, 233–248 (1972)
14. Lam, D.C.C., Yang, F., Chong, A.C.M., Wang, J., Tong, P.: Experiments and theory in strain gradient elasticity. J. Mech. Phys. Solids. **51**, 1477–1508 (2003)
15. Ejike, U.B.C.O.: The plane circular crack problem in the linearized couple-stress theory. Int. J. Eng. Sci. **7**, 947–961 (1969)
16. Yang, F., Chong, A.C.M., Lam, D.C.C., Tong, P.: Couple stress based strain gradient theory for elasticity. Int. J. Solids Struct. **39**, 2731–2743 (2002)
17. Rafii-Tabar, H., Shodja, H.M., Darabi, M., Dahi, A.: Molecular dynamics simulation of crack propagation in fcc materials containing clusters of impurities. Mech. Mater. **38**, 243–252 (2006)
18. Tadi Beni, Y., Karimipöur, I., Abadyan, M.R.: Modeling the effect of intermolecular force on the size-dependent pull-in behavior of beam-type NEMS using modified couple stress theory. J. Mech. Sci. Technol. **28**, 3749–3757 (2014)
19. Karimipöur, I., Tadi Beni, Y., Koochi,A., Abadyan, M.R.: Using couple stress theory for modeling the size-dependent instability of double-sided beam-type nanoactuators in the presence of Casimir force. J Braz. Soc. Mech. Sci. Eng. (2015). doi:10.1007/s40430-015-0385-6
20. Tadi Beni, Y., Karimipöur, I., Abadyan, M.R.: Modeling the instability of electrostatic nano-bridges and nano-cantilevers using modified strain gradient theory. Appl. Math. Model. **39**, 2633–2648 (2015)
21. Karimipöur, I., Kanani, A., Koochi, A., Keivani, M., Abadyan, M.: Modeling the electromechanical behavior and instability threshold of NEMS bridge in electrolyte considering the size dependency and dispersion forces. Phys. E **74**, 140–150 (2015)
22. Wang, W., Huang, Y., Hsia, K.J., Hu, K.X., Chandra, A.: A study of microbend test by strain gradient plasticity. Int. J. Plast. **19**, 365–382 (2003)
23. Mindlin, R.D.: Micro-structure in linear elasticity. Arch. Ration. Mech. Anal. **16**, 51–78 (1964)
24. Mindlin, R.D.: Second gradient of strain and surface-tension in linear elasticity. Int. J. Solids Struct. **1**, 417–438 (1965)
25. Mindlin, R.D.: Influence of couple-stresses on stress concentrations. Exp. Mech. **3**, 1–7 (1963)
26. Lubarda, V.A.: The effect of couple stresses on dislocation strain energy. Int. J. Solids Struct. **40**, 3807–3826 (2003)
27. Shodja, H.M., Ghazisaeidi, M.: Effects of couple stresses on anti-plane problems of piezoelectric media with inhomogeneities. Eur. J. Mech. A. Solids. **26**, 647–658 (2007)
28. Haftbaradaran, H., Shodja, H.M.: Elliptic inhomogeneities and inclusions in anti-plane couple stress elasticity with application to nano-composites. Int. J. Solids Struct. **46**, 2978–2987 (2009)

29. Zhang, X., Jiao, K., Sharma, P., Yakobson, B.I.: An atomistic and non-classical continuum field theoretic perspective of elastic interactions between defects (force dipoles) of various symmetries and application to grapheme. J. Mech. Phys. Solids. **54**, 2304–2329 (2006)
30. Shodja, H.M., Tehranchi, A.: A formulation for the characteristic lengths of fcc materials in first strain gradient elasticity via the Sutton–Chen potential. Philos. Mag. **90**, 1893–1913 (2010)
31. Shodja, H.M., Davoudi, K.M., Gutkin, MYu.: Analysis of displacement and strain fields of a screw dislocation in a nanowire using gradient elasticity theory. Scr. Mater. **59**, 368–371 (2008)
32. Davoudi, K.M., Gutkin, MYu., Shodja, H.M.: Analysis of stress field of a screw dislocation inside an embedded nanowire using strain gradient elasticity. Scr. Mater. **61**, 355–358 (2009)
33. Aifantis, E.C.: A note on gradient elasticity and nonsingular crack fields. J. Mech. Behav. Mater. **20**, 103–105 (2011)
34. Aifantis, E.C.: On the gradient approach—relation to Eringen's nonlocal theory. Int. J. Eng. Sci. **49**, 1367–1377 (2011)
35. Aifantis, E.C.: On non-singular gradela crack fields. Theor. Appl. Mech. Lett **4**, 051005 (2014)
36. Lazar, M., Polyzos, D.: On non-singular crack fields in Helmholtz type enriched elasticity theories. Int. J. Solids Struct. **62**, 1–7 (2015)
37. Gutkin, M.Yu., Aifantis, E.C.: Edge dislocation in gradient elasticity. Scdpta Mater. **36**, 129–135 (1997)
38. Aifantis, E.C.: Update on a class of gradient theories. Mech. Mater. **35**, 259–280 (2003)
39. Paulino, G.H., Fannjiang, A.C., Chan, Y.S.: Gradient elasticity theory for mode III fracture in functionally graded materials—part I: crack perpendicular to the material gradation. ASME J. Appl. Mech. **70**, 531–542 (2003)
40. Chan, Y.S., Paulino, G.H., Fannjiang, A.C.: Gradient elasticity theory for mode III fracture in functionally graded materials—part II: crack parallel to the material gradation. ASME J. Appl. Mech. **75**, 061015 (2008)
41. Georgiadis, H.G.: The mode III crack problem in micro structured solids governed by dipolar gradient elasticity: static and dynamic analysis. J. Appl. Mech. **70**, 517–530 (2003)
42. Chan, Y.S., Fannjiang, A.C., Paulino, G.H.: Integral equations with hypersingular kernels theory and application to fracture mechanics. Int. J. Eng. Sci. **41**, 683–720 (2003)
43. Casal, P.: La théorie du second gradient et la capillarité. C.R. Acad. Sci. Paris A. **274**, 1571–1574 (1972)
44. Unger, D.J., Aifantis, E.C.: Strain gradient elasticity theory for antiplane shear cracks. Part II: monotonic displacements. Theor. Appl. Fract. Mech. **3**, 253–265 (2000)
45. Vardoulakis, I.: Degradation and Instabilities in Geomaterials, (Chapter 3: Linear Micro-elasticity). CISM International Centre for Mechanical Sciences (2004)
46. Fannjiang, A.C., Chan, Y.S., Paulino, G.H.: Strain-gradient elasticity for mode III cracks: a hypersingular integrodifferential equation approach. SIAM J. Appl. Math. **62**, 1066–1091 (2002)
47. Askes, H., Aifantis, E.C.: Gradient elasticity in statics and dynamics: an overview of formulations, length scale identification procedures, finite element implementations and new results. Int. J. Solids Struct. **48**, 1962–1990 (2011)
48. Exadaktylos, G., Vardoulakis, I.: Bifurcations, Instabilities, Degradation in Geomechanics. Springer, Berlin (2007)
49. Vardoulakis, I.G., Sulem, J.: Bifurcation Analysis in Geomechanics, Blackie Academic and Professional. CRC Press, Boca Raton (1995)
50. Gourgiotis, P.A., Georgiadis, H.G.: Distributed dislocation approach for cracks in couple-stress elasticity: shear modes. Int. J. Fract. **147**, 83–102 (2007)
51. Altan, S., Aifantis, E.: On the structure of the mode III crack-tip in gradient elasticity. Scr. Metall. Mater. **26**, 319–324 (1992)
52. Ru, C., Aifantis, E.: A simple approach to solve boundary-value problems in gradient elasticity. Acta Mech. **101**, 59–68 (1993)
53. Faal, R.T., Fotuhi, A.R., Fariborz, S.J., Daghyani, H.R.: Anti-plane stress analysis of an isotropic wedge with multiple cracks. Int. J. Solids Struct. **41**, 4535–4590 (2004)
54. Fotuhi, A.R., Fariborz, S.J.: Anti-plane analysis of a functionally graded strip with multiple cracks. Int. J. Solids Struct. **43**, 1239–1252 (2006)
55. Wen, P.H., Aliabadi, M.H., Rooke, D.P.: Dynamic analysis of mode III cracks in rectangular sheets. Int. J. Fract. **80**, R37–R41 (1989)
56. Fotuhi, A.R., Fariborz, S.J.: In-plane stress analysis of an orthotropic plane containing multiple defects. Int. J. Solids Struct. **44**, 4167–4183 (2007)
57. Hills, D.A., Kelly, P.A., Dai, D.N., Korsunsky, A.M.: Solution of Crack Problems: The Distributed Dislocation Technique. Kluwer Academic Publishers, Amsterdam (1996)
58. Korsunsky, A.M., Hills, D.A.: The solution of crack problems by using distributed strain nuclei. Proc. Inst. Mech. Eng. Part C. J. Mech. Eng. Sci. **210**, 23–31 (1996)
59. Erdogan, F., Gupta, G.D., Cook, T.S.: Numerical solution of integral equations. In: Sih, G.C. (ed.) Methods of Analysis and Solution of Crack Problems, vol. 1, pp. 368–425. Noord hoof, Leyden (1973)
60. Abramowitz, M., Stegun, I.A.: Handbook of Mathematical Function. Dover, New York (1965)
61. Baghestani, A.M., Fotuhi, A.R., Fariborz, S.J.: Multiple interacting cracks in an orthotropic layer. Arch. Appl. Mech. **83**, 1549–1567 (2013)
62. Tada, H., Paris, P.C., Irwin, G.R.: The Stress Analysis of Cracks Handbook, 3rd edn. ASME Press, Del Research Corporation, Hellertown (2000)
63. Fotuhi, A.R., Fariborz, S.J.: Stress analysis in a wedge weakened by multiple cracks. Int. J. Mech. Sci. **70**, 113–129 (2013)
64. Mousavi, S.M.: Dislocation-based fracture mechanics within nonlocal and gradient elasticity of bi-Helmholtz type—part I: antiplane analysis. Int. J. Solids Struct. **87**, 222–235 (2016)
65. Vardoulakis, I., Exadaktylos, G., Aifantis, E.C.: Gradient elasticity with surface energy: mode III crack problem. Int. J. Solids Struct. **33**, 4531–4559 (1996)
66. Exadaktylos, G., Vardoulakis, I., Aifantis, E.C.: Cracks in gradient elastic bodies with surface energy. Int. J. Fract. **79**, 107–119 (1996)
67. Mousavi, S.M., Aifantis, E.C.: A note on dislocation-based mode III gradient elastic fracture mechanics. J. Mech Behav. Mater. **24**, 115–119 (2015)

68. Fleck, N.A., Muller, G.M., Ashby, M.F., Hutchinson, J.W.: Strain gradient plasticity: theory and experiment. Acta Metall. Mater. **42**, 475–487 (1994)
69. Stolken, J.S., Evans, A.G.: A microbend test method for measuring the plasticity length scale. Acta Mater. **46**, 5109–5115 (1998)
70. Chong, A.C.M., Lam, D.C.C.: Strain gradient plasticity effect in indentation hardness of polymers. J. Mater. Res. **14**, 4103–4110 (1999)
71. Cao, Y., Nankivil, D.D., Allameh, S., Soboyejo, W.O.: Mechanical properties of Au films on silicon substrates. Mater. Manuf. Process. **22**, 187–194 (2007)
72. Wang, W., Huang, Y., Hsia, K.J., Hu, K.X., Chandra, A.: A study of microbend test by strain gradient plasticity. Int. J. Plast. **19**, 365–382 (2003)